






## Effect of a soluble surfactant on the linear stability of two-phase flows in a finite-length channel

M. A. Herrada <sup>1</sup>, A. Ponce-Torres,<sup>2</sup> P. R. Kaneelil <sup>3</sup>, A. A. Pahlavan <sup>4</sup>,  
H. A. Stone <sup>3</sup> and J. M. Montanero <sup>2</sup>

<sup>1</sup>*Departamento de Ingeniería Aeroespacial y Mecánica de Fluidos, Universidad de Sevilla, E-41092 Sevilla, Spain*

<sup>2</sup>*Departamento de Ingeniería Mecánica, Energética y de los Materiales and Instituto de Computación Científica Avanzada (ICCAEx), Universidad de Extremadura, E-06006 Badajoz, Spain*

<sup>3</sup>*Department of Mechanical and Aerospace Engineering, Princeton University, Princeton, New Jersey 08544, USA*

<sup>4</sup>*Department of Mechanical Engineering and Material Science, Yale University, New Haven, Connecticut 06511-8286, USA*



(Received 11 July 2022; accepted 8 November 2022; published 28 November 2022)

We study numerically the effect of a soluble surfactant on the stability of two-phase flow in a finite-length microchannel. We calculate the steady base flow and its global eigenmodes for experimentally relevant choices of material, kinetic, and flow parameters. The results show that the system is unstable for capillary numbers above a critical value. The surfactant surface concentration takes values of the order of the maximum packing density over the whole interface, even for very small volume concentrations. The two streams drag the surfactant molecules toward the downstream end of the interface against the action of the Marangoni stress. The sharp reduction of the interfacial tension at that end enhances the interface deformation and considerably destabilizes the system, translating into a sharp reduction of the critical capillary number.

DOI: [10.1103/PhysRevFluids.7.114003](https://doi.org/10.1103/PhysRevFluids.7.114003)

### I. INTRODUCTION

Numerous microfluidic applications involve two immiscible fluids moving side by side in microchannels. This configuration has been used to produce chemical reactions [1–5], mass transfer, and separation of species [6,7], among other phenomena (see, e.g., Refs. [1–9] in Ref. [8]). The stability conditions for these two-phase flows are well established in the case of infinitely long microchannels [9–11]. However, much less is known when the interface is constrained between the two ends of a channel of finite length, a relevant configuration in many applications.

In a two-phase flow in a microchannel of finite length, two immiscible streams are injected into their respective inlet ducts and brought into contact at the junction. These streams move parallel along the microchannel, separated by an interface pinned to the channel ends. Finally, the two phases are separated at the exit and flow across two outlet ducts. On many occasions, there is undesirable leakage of one phase into the outlet duct of the other. It is believed that this imperfect separation is caused by a difference between the viscous pressure drops through the inlet ducts due to an imperfect symmetry of the microfluidic device or a mismatch of the viscosities and injection flow rates. The difference between the pressure drops is balanced by the capillary pressure produced by the interface deformation. If the pressure drop difference exceeds a certain critical value, the interface destabilizes and breaks up or depins from the channel ends, allowing one phase to penetrate into the duct carrying the other.

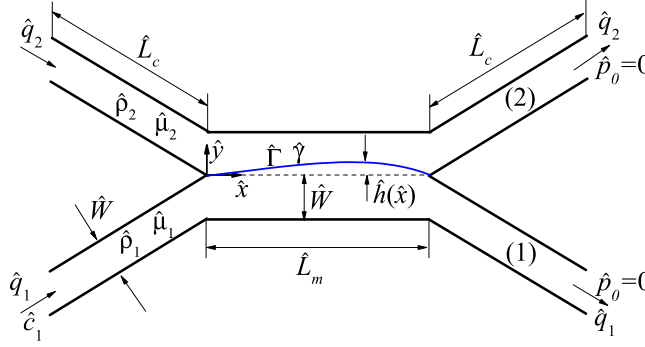


FIG. 1. Sketch of the fluid configuration.

Most of the previous works have focused on proposing strategies to stabilize the system and solve or mitigate the practical problem described above [12–15]. Very recently, the physical mechanism underlying this instability has been investigated both theoretically and experimentally [8]. The results show that this instability is localized near the channel exit, where a “bump” of one of the phases grows over time and protrudes into the other phase stream. This process leads to the periodic shedding of droplets of one fluid into the other with a frequency proportional to the flow rate. The study revealed the extreme sensitivity of this flow system to the device asymmetry and viscosity difference.

Many of the applications of two-phase flows in microchannels involve liquids in which surfactants are dissolved. The interfacial tension opposes the instability mechanism described above. Therefore, the presence of a surfactant monolayer is expected to affect that mechanism. Apart from the obvious effect associated with the global decrease in the interfacial tension, there may be a complex interplay between the local reduction of this quantity (the soluto-capillarity effect) and Marangoni convection. In fact, surfactant molecules adsorbed onto the interface are expected to be dragged by the two coflowing streams toward the microchannel end, where instability is localized. The extra reduction of the interfacial tension in that region can significantly alter the critical conditions and how the system evolves after the instability is triggered.

In this paper, we examine the global stability of the fluid configuration described above when one of the two phases transports a dissolved surfactant. The results show that the system becomes unstable for capillary numbers exceeding a critical value. We analyze how the surfactant affects the critical conditions and the growth of the small-amplitude perturbations responsible for the instability.

## II. FORMULATION OF THE PROBLEM

We analyze numerically the effect of a soluble surfactant on the stability of the two-phase flow sketched in Fig. 1. The microfluidic device consists of two identical two-dimensional (2D) channels (1 and 2) of length  $\hat{L}_c$  and width  $\hat{W}$ , joining with an angle  $\alpha$  at the entrance. The length and width of the junction are  $\hat{L}_m$  and  $2\hat{W}$ , respectively. In the experiments that motivated the present analysis [8], the typical length scale in the third direction was  $\mathcal{O}(100) \mu\text{m}$ , with the largest being  $750 \mu\text{m}$ . The system was three-dimensional (3D), and the pressure set by the interface curvature into the plane was important and was a focus of that work. Nevertheless, the 2D simulations were in qualitative agreement with the experiments. Because of the challenge of 3D simulations with surfactant transport, it is natural to learn from the 2D simulations reported here.

A liquid of density  $\hat{\rho}_1$  ( $\hat{\rho}_2$ ) and viscosity  $\hat{\mu}_1$  ( $\hat{\mu}_2$ ) is injected at a constant flow rate  $\hat{q}_1$  ( $\hat{q}_2$ ) across channel 1 (2). We assume that both streams discharge into a common reservoir and therefore are at the same pressure  $\hat{p}_o = 0$ . The function  $\hat{y} = \hat{h}(\hat{x}, t)$  indicates the interface location in the Cartesian coordinate system  $(\hat{x}, \hat{y})$  shown in Fig. 1. The interface is anchored at the points (0,0) and (0,  $\hat{L}_m$ ). In the absence of surfactant, the interfacial tension is  $\hat{\gamma}_0$ .

We examine the effect on the flow stability of a surfactant dissolved in phase 1. The surfactant transport is described in terms of the bulk and surface diffusion coefficients,  $\hat{\mathcal{D}}_1$  and  $\hat{\mathcal{D}}_s$ , as well as the parameters involved in the interface kinetic model for the net adsorption/desorption flux,

$$\hat{\mathcal{J}} = \hat{k}_a \hat{c} \left( 1 - \frac{\hat{\Gamma}}{\hat{\Gamma}_\infty} \right) - \hat{k}_d \hat{\Gamma}. \quad (1)$$

In this equation,  $\hat{k}_a$  and  $\hat{k}_d$  are the adsorption and desorption constants, respectively,  $\hat{c}$  is the bulk surfactant concentration evaluated at the interface, and  $\hat{\Gamma}_\infty$  is the maximum packing density. The effect of the surfactant surface concentration  $\hat{\Gamma}$  on the interfacial tension  $\hat{\gamma}$  is described by the Langmuir equation of state [16],

$$\hat{\gamma} = \hat{\gamma}_0 + \hat{\Gamma}_\infty \hat{R}_g \hat{T} \ln \left( 1 - \frac{\hat{\Gamma}}{\hat{\Gamma}_\infty} \right), \quad (2)$$

where  $\hat{R}_g$  is the gas constant and  $\hat{T}$  is the temperature. Equation (1) yields the Langmuir equation at equilibrium for  $\hat{\mathcal{J}} = 0$  [17],

$$\frac{\hat{c}}{\hat{k}_d / \hat{k}_a} = \frac{\hat{\Gamma} \hat{\Gamma}_\infty}{\hat{\Gamma}_\infty - \hat{\Gamma}}. \quad (3)$$

The combination of Eq. (3) and the Gibbs isotherm [18]

$$\hat{\Gamma} = - \frac{1}{\hat{R}_g \hat{T}} \left( \frac{\partial \hat{\gamma}}{\partial \ln \hat{c}} \right)_{\hat{T}, \hat{p}} \quad (4)$$

leads to Eq. (2).

We neglect the effect of the surfactant surface viscosity because of the nearly inviscid character of most soluble surfactants, such as sodium dodecyl sulfate (SDS) [19]. In fact, the surface viscosity of this type of surfactant becomes relevant only for very high surface velocity gradients, such as those arising in the pinch-off of interfaces [20] or tip streaming [21]. The surfactant is convected throughout the incompressible liquid phase 1. For this reason, the surfactant concentration at the inlet of channel 1 is approximately the same as that in the reservoir,  $\hat{c}_1 = \hat{c}_\infty$ . We assume that the bulk surfactant concentration is smaller than the critical micellar concentration  $\hat{c}_{cmc}$  and therefore micelles are not formed.

The bulk diffusion coefficient  $\hat{\mathcal{D}}_1$  corresponds to very high values of the Peclet number in most experiments. This implies that the bulk surfactant concentration is almost uniform except within a very thin diffusive layer formed next to the interface. The scale of the diffusive layer thickness  $\hat{\lambda}_D$  can be estimated from the expression

$$\hat{\mathcal{D}}_1 \hat{c}_\infty / \hat{\lambda}_D \approx \hat{k}_a \hat{c}_\infty. \quad (5)$$

For the values of  $\hat{\mathcal{D}}_1$ ,  $\hat{k}_a$ , and  $\hat{W}$  considered in this work,  $\hat{\lambda}_D / \hat{W} \approx 10^{-2}$ . The disparity between the thickness of the diffusive layer formed next to the interface and the channel width poses a major challenge to the numerical simulation.

We choose the channel width  $\hat{W}$ , visco-capillary velocity  $\hat{U}_\mu = \hat{\gamma}_c / \hat{\mu}_1$  ( $\hat{\gamma}_c$  is a characteristic value of  $\hat{\gamma}$  defined below), and capillary pressure  $\hat{\mu}_1 \hat{U}_\mu / \hat{W}$  as characteristic length, velocity, and pressure, respectively. In the absence of surfactants, the problem can be formulated in terms of the density

TABLE I. Dimensionless parameters and their physical meaning.

Parameter	Physical meaning	Definition
$\rho$	Upper density/lower density	$\hat{\rho}_2/\hat{\rho}_1$
$\mu$	Upper viscosity/lower viscosity	$\hat{\mu}_2/\hat{\mu}_1$
Oh	Inertio-capillary Reynolds number	$\frac{\hat{\mu}_1^2}{\hat{\rho}_1 \hat{W} \hat{\gamma}_{eq}}$
$Ca$	Lower viscosity/interfacial tension	$\frac{\hat{q}_1 \hat{\mu}_1}{\hat{W} \hat{\gamma}_{eq}}$
$q$	Upper flow rate/lower flow rate	$\hat{q}_2/\hat{q}_1$
Pe	Surfactant volumetric convection/diffusion	$\frac{\hat{W} \hat{\gamma}_{eq}}{\hat{\mu}_1 \hat{D}_1}$
$Pe_s$	Surfactant surface convection/diffusion	$\frac{\hat{W} \hat{\gamma}_{eq}}{\hat{\mu}_1 \hat{D}_{s1}}$
$k_a$	Adsorption rate	$\frac{\hat{k}_a \hat{c}_{cmc} \hat{W} \hat{\mu}_1}{\hat{\Gamma}_\infty \hat{\gamma}_{eq}}$
$k_d$	Desorption rate	$\frac{\hat{k}_d \hat{W} \hat{\mu}_1}{\hat{\gamma}_{eq}}$
Ma	Surfactant strength	$\frac{\hat{\Gamma}_\infty \hat{R}_g \hat{T}}{\hat{\gamma}_{eq}}$
$c_\infty$	Reservoir surfactant concentration	$\hat{c}_\infty/\hat{c}_{cmc}$

and viscosity ratios,  $\rho = \hat{\rho}_2/\hat{\rho}_1$  and  $\mu = \hat{\mu}_2/\hat{\mu}_1$ , the Ohnesorge and capillary numbers,

$$\text{Oh} = \frac{\hat{\mu}_1}{\hat{\rho}_1 \hat{U}_\mu \hat{W}} = \frac{\hat{\mu}_1^2}{\hat{\rho}_1 \hat{W} \hat{\gamma}_c} \quad \text{and} \quad Ca = \frac{\hat{q}_1}{\hat{W} U_\mu} = \frac{\hat{q}_1 \hat{\mu}_1}{\hat{W} \hat{\gamma}_c}, \quad (6)$$

and the flow rate ratio  $q = \hat{q}_2/\hat{q}_1$ .

When a soluble surfactant is added to phase 1, the following additional dimensionless numbers are considered: The bulk and surface Peclet numbers,  $\text{Pe} = \hat{W} \hat{U}_\mu / \hat{D}_1$  and  $\text{Pe}_s = \hat{W} \hat{U}_\mu / \hat{D}_{s1}$ , the dimensionless adsorption and desorption constants,  $k_a = \hat{k}_a \hat{c}_{cmc} \hat{W} / (\hat{\Gamma}_\infty \hat{U}_\mu)$  and  $k_d = \hat{k}_d \hat{W} / \hat{U}_\mu$ , the (Marangoni) elasticity number  $\text{Ma} = \hat{\Gamma}_\infty \hat{R}_g \hat{T} / \hat{\gamma}_c$ , and the reservoir surfactant concentration  $c_\infty = \hat{c}_\infty / \hat{c}_{cmc}$ .

In a typical experimental run, the system properties are fixed, and the flow rates are progressively increased in the same proportion. With the choice of the visco-capillary velocity  $U_\mu$  as a characteristic quantity (instead of the convective velocity  $\hat{q}_1/\hat{W}$ ), the experimental run corresponds to increasing the capillary number while the rest of the dimensionless numbers are fixed.

The most obvious surfactant effect on the flow stability is the global reduction of interfacial tension. To eliminate this effect from our analysis, we choose the equilibrium interfacial tension  $\hat{\gamma}_{eq}$  (instead of  $\hat{\gamma}_0$ ) as the characteristic value  $\gamma_c$ . The interfacial tension  $\hat{\gamma}_{eq}$  can be calculated from Eqs. (2) and (3) as a function of the surfactant concentration  $\hat{c}_\infty$ . Consider a fluid-fluid system with a clean interface and another with the same densities and viscosities but with an interface loaded with a surfactant monolayer producing the same equilibrium interfacial tension. These two systems may behave differently due to the inhomogeneity of the interfacial tension when the surfactant monolayer is present. With the choice  $\hat{\gamma}_c = \hat{\gamma}_{eq}$ , they are characterized by the same values of the dimensionless numbers except for  $c_\infty$ . Therefore, the dimensionless surfactant concentration  $c_\infty$  quantifies the effects of local soluto-capillarity and Marangoni convection (not the global reduction of interfacial tension).

For a fixed geometry, the set of dimensionless numbers becomes  $\{\rho, \mu, \text{Oh}, Ca, q; \text{Pe}, \text{Pe}_s, k_a, k_d, \text{Ma}, c_\infty\}$  (Table I). For a given pair of liquids and a given surfactant, the only independent variables are  $Ca$  and  $q$ . We will study the instabilities that occur when  $Ca$  reaches a critical value for fixed values of the rest of the dimensionless parameters.

### III. GOVERNING EQUATIONS AND NUMERICAL METHOD

Hereafter, all the variables are made dimensionless using the characteristic quantities mentioned above. The Navier-Stokes equations for the 2D velocity  $\mathbf{v}^{(k)}(x, y; t)$  and pressure  $p^{(k)}(x, y; t)$  fields are

$$u_x^{(k)} + v_y^{(k)} = 0, \quad (7)$$

$$\text{Oh}^{-1} \rho^{\delta_{k2}} (u_t^{(k)} + u^{(k)} u_x^{(k)} + v^{(k)} u_y^{(k)}) = -p_x^{(k)} + \mu^{\delta_{k2}} (u_{xx}^{(k)} + u_{yy}^{(k)}), \quad (8)$$

$$\text{Oh}^{-1} \rho^{\delta_{k2}} (v_t^{(k)} + u^{(k)} v_x^{(k)} + v^{(k)} v_y^{(k)}) = -p_y^{(k)} + \mu^{\delta_{k2}} (v_{xx}^{(k)} + v_{yy}^{(k)}), \quad (9)$$

where  $t$  is the time,  $x$  and  $y$  are the Cartesian coordinates,  $u^{(k)}$  and  $v^{(k)}$  are the corresponding velocity components for phase  $k$ , and  $\delta_{ij}$  is the Kronecker delta. In the above equations and henceforth, the superscripts  $k = 1$  and  $2$  indicate the phase where the variable is evaluated. In addition, subscripts  $t$ ,  $x$ , and  $y$  denote the partial derivatives with respect to the corresponding variables. The action of the gravitational field has been neglected due to the smallness of the fluid configuration and the corresponding Bond number.

We assume that the surfactant molecules are dissolved in phase 1 as monomers at a concentration below the critical micellar concentration. In this case, the surfactant volumetric concentration  $c^{(1)}(x, y; t)$  (measured in terms of the critical micellar concentration  $\hat{c}_{\text{cmc}}$ ) is calculated from the conservation equation [22,23]

$$c_t^{(1)} + u^{(1)} c_x^{(1)} + v^{(1)} c_y^{(1)} = \text{Pe}^{-1} (c_{xx}^{(1)} + c_{yy}^{(1)}). \quad (10)$$

The kinematic compatibility and the velocity field continuity at the interface  $y = h(x, t)$  yields

$$h_t + h_x u^{(1)} - v^{(1)} = 0, \quad u^{(1)} = u^{(2)}, \quad v^{(1)} = v^{(2)}. \quad (11)$$

The equilibrium of both tangential and normal stresses, respectively, leads to

$$|4\mu^{\delta_{k2}} h_x u_x^{(k)} + \mu^{\delta_{k2}} (h_x^2 - 1) (u_y^{(k)} + v_x^{(k)})|_2 = -\gamma_x \sqrt{1 + h_x^2}, \quad (12)$$

$$|-p^{(k)} (1 + h_x^2) + 2\mu^{\delta_{k2}} [h_x^2 u_x^{(k)} + v_y^{(k)} - h_x (u_y^{(k)} + v_x^{(k)})]|_2 = \frac{\gamma h_{xx}}{\sqrt{1 + h_x^2}}, \quad (13)$$

where  $|A|_2 \equiv A^{(1)} - A^{(2)}$  and  $\gamma = \hat{\gamma} / \hat{\gamma}_{\text{eq}}$ .

The dependence of the interfacial tension  $\gamma$  upon the surfactant surface concentration is calculated from the Langmuir equation of state 2 [16], which in dimensionless form is

$$\gamma = 1 + \text{Ma} \ln \left( \frac{1 - \Gamma}{1 - \Gamma_{\text{eq}}} \right), \quad (14)$$

where  $\Gamma = \hat{\Gamma} / \hat{\Gamma}_{\infty}$  is the reduced surfactant surface density, and  $\Gamma_{\text{eq}} = \hat{\Gamma}_{\text{eq}} / \hat{\Gamma}_{\infty}$  is the value corresponding to the equilibrium surface concentration  $\hat{\Gamma}_{\text{eq}}$ .

The reduced surfactant surface density is calculated by integrating the conservation equation

$$\Gamma_t + \frac{\Gamma v_x^t}{\sqrt{1 + h_x^2}} + \frac{\Gamma_x v^t}{\sqrt{1 + h_x^2}} - \frac{\Gamma v'' h_{xx}}{\sqrt{1 + h_x^2}} = \frac{1}{\text{Pe}_s} \frac{1}{\sqrt{1 + h_x^2}} \left( \frac{\Gamma_x}{\sqrt{1 + h_x^2}} \right)_x + \mathcal{J}, \quad (15)$$

where

$$v^t = \frac{u^{(k)} + h_x v^{(k)}}{\sqrt{1 + h_x^2}} \quad \text{and} \quad v^n = \frac{-h_x u^{(k)} + v^{(k)}}{\sqrt{1 + h_x^2}} \quad (16)$$

are the tangential and normal velocity components at the interface, respectively, while  $\mathcal{J} = \hat{\mathcal{J}}/(\hat{U}_\mu \hat{\Gamma}_\infty / \hat{W})$  is the net flux of surfactant given by the expression [Eq. (1)] [17,22,23]

$$\mathcal{J} = k_a c(1 - \Gamma) - k_d \Gamma. \quad (17)$$

This flux equals the surfactant diffused from/to the bulk, i.e.,

$$\mathcal{J} = \frac{c_x h_x - c_y}{\text{Pe} \sqrt{1 + h_x^2}} \Big|_{y=h(x,t)}. \quad (18)$$

This equation couples surfactant transport across the bulk and at the interface.

Parabolic velocity profiles with mean velocities  $U_1 = Ca$  and  $U_2 = qCa$  were prescribed at the inlet of channels 1 and 2, respectively. The outflow condition  $p^{(k)} = 0$  was imposed at the outlet sections. The no-slip boundary condition was considered in all the solid walls. The triple contact line was anchored at the two ends of the interface, i.e.,  $h = 0$  at  $x = 0$  and  $L_m$  ( $L_m = \hat{L}_m / \hat{W}$ ). The reservoir surfactant concentration  $c_\infty$  is imposed at the inlet section of channel 1. The surfactant concentration at the inlet section of channel 2 is zero and remains zero in phase 2 for all time. The numerical integration of Eq. (15) is performed considering zero diffusive surfactant flux at the location of the triple contact lines.

In the global stability analysis, we assume the temporal dependence

$$\begin{aligned} U(x, y; t) &= U_0(x, y) + \delta U(x, y) e^{-i\omega t} + \text{c.c.} \quad (|\delta U| \ll |U_0|), \\ h(x; t) &= h_0(x) + \delta h(x) e^{-i\omega t} + \text{c.c.} \quad (|\delta h| \ll h_0) \\ \Gamma(x; t) &= \Gamma_0(x) + \delta \Gamma(x) e^{-i\omega t} + \text{c.c.} \quad (|\delta \Gamma| \ll \Gamma_0) \end{aligned} \quad (19)$$

where  $U$  represents the velocity, pressure, and bulk surfactant concentration fields, while  $U_0$  and  $\delta U$  stand for the base flow (steady) solution and the spatial dependence of the eigenmode, respectively. In addition,  $h_0$  and  $\Gamma_0$  represent the base flow solution for  $h$  and  $\Gamma$ , respectively,  $\delta h$  and  $\delta \Gamma$  are the corresponding perturbation amplitudes and c.c. denotes complex conjugate. The perturbation evolves according to the eigenfrequency  $\omega = \omega_r + i\omega_i$ , where  $\omega_r$  and  $\omega_i$  are the oscillation frequency and growth rate, respectively. Eigenmodes with  $\omega_i < 0$ ,  $\omega_i = 0$ , and  $\omega_i > 0$  correspond to damped, marginally stable, and unstable perturbations, respectively.

The global surfactant mass conservation condition,

$$\int_0^{L_m} \sqrt{1 + h_{0x}^2} \mathcal{J}_0 dx = 0, \quad (20)$$

is taken into account when calculating the base (steady) flow.

The governing equations are integrated with a variant of the numerical method proposed by Herrada and Montanero [24]. As mentioned in Sec. II, the major difficulty associated with the presence of soluble surfactants is the existence of a very thin diffusive layer next to the interface for the small bulk diffusion coefficient of most surfactants. However, the discretization in the direction transverse to the flow with Chebyshev spectral collocation points accumulates the grid points next to the interface [24], which facilitates the resolution of the diffusive boundary layer.

The method described by Herrada and Montanero [24] allows one to obtain both the base flow and its eigenmodes. It can be seen that the calculation of the eigenmodes involves the Jacobian of the system evaluated with the base solution. The matrix accounting for the temporal dependence of the problem is calculated with essentially the same procedure as that for the Jacobian. Ponce-Torres *et al.* [25] explained this technical aspect of the problem in some detail.

For the sake of illustration, Fig. 2 shows the eigenfrequencies with  $\omega_i \geq -8.42 \times 10^{-4}$  for a subcritical and supercritical capillary number. The growth rate  $\omega_i$  becomes positive, and the base flow becomes unstable when the capillary number exceeds a critical value. The stability transition can be easily identified: A slight change in the capillary number significantly increases the dominant

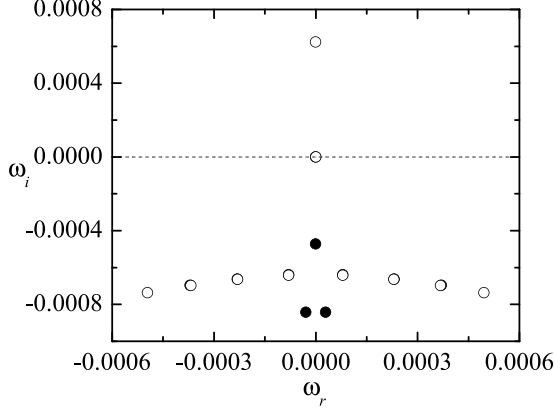


FIG. 2. Growth rate  $\omega_i$  and frequency  $\omega_r$  of the eigenvalues with  $\omega_i \geq -8.42 \times 10^{-4}$  for  $Ca = 0.00681$  (solid symbols) and  $Ca = 0.00690$  (open symbols). The results were calculated for  $\{\rho = 1.72, \mu = 0.5, Oh = 0.00141, q = 1; Pe = Pe_s = 3.54 \times 10^6, k_a = 5.96 \times 10^{-6}, k_d = 5.37 \times 10^{-9}, Ma = 0.225, c_\infty = 0.0055\}$ .

mode growth rate. The critical capillary number  $Ca^*$  is calculated as the average value between the subcritical and supercritical ones ( $Ca^* \simeq 0.00686$ ).

#### IV. RESULTS

We choose the values of the geometrical parameters  $\hat{L}_c = 6$  mm,  $\hat{L}_m = 12$  mm,  $\hat{W} = 0.75$  mm, and  $\alpha = 45^\circ$ . These values are the same as those considered in the experimental study of Kaneelil *et al.* [8] except for the length of the outlet channels, which are shorter in our work. The properties of the liquids approximately correspond to those of 50.5% glycerol in water and perfluorodecalin also considered by Kaneelil *et al.* [8]:  $\hat{\rho}_1 = 1124$  kg/m<sup>3</sup>,  $\hat{\rho}_2 = 1930$  kg/m<sup>3</sup>,  $\hat{\mu}_1 = 5.6$  mPa s,  $\hat{\mu}_2 = 5.6$  mPa s, and  $\hat{\gamma}_0 = 38$  mN/m. Kaneelil *et al.* [8] conducted most of their experiments in the absence of any added surfactant. We take the surfactant properties considered by Kalogirou and Blyth [23] as a reference:  $\hat{D}_1 = \hat{D}_s = 5.5 \times 10^{-10}$  m<sup>2</sup>/s,  $\hat{\Gamma}_\infty = 2.4$   $\mu$ mol/m<sup>2</sup>,  $\hat{R}_g = 8.314$  J/(K mol),  $\hat{T} = 298.15$  K,  $\hat{k}_a = 10^{-5}$  m/s,  $\hat{k}_d = 3.38 \times 10^{-5}$  s<sup>-1</sup>, and  $\hat{c}_{cmc} = 9 \times 10^{-3}$  mol/m<sup>3</sup>. To facilitate the convergence in the simulations, we consider smaller values of  $\hat{\mu}_2$  and slightly increase the diffusion coefficient,  $\hat{D}_1 = \hat{D}_s = 10^{-9}$  m<sup>2</sup>/s. The above values lead to the following dimensionless numbers for the reference case:  $\rho = 1.72$ ,  $Oh = 0.00141$ ,  $Pe = Pe_s = 3.54 \times 10^6$ ,  $k_a = 5.96 \times 10^{-6}$ ,  $k_d = 5.37 \times 10^{-9}$ , and  $Ma = 0.225$ . We will conduct simulations for different values of the viscosity ratio  $\mu$ .

The interface deformation and surfactant volume concentration of the base flow when a small amount of surfactant is added to phase 1 is shown in Fig. 3. The figure also shows the interface deformation without surfactant for the same values of  $\rho$ ,  $\mu$ ,  $Oh$ ,  $q$ , and  $Ca$ . The flow drags the surfactant molecules over the interface, increasing the surfactant surface concentration in the vicinity of the right-hand interface end. This reduces the interfacial tension there, shifting the maximum interfacial deformation towards the right-hand anchorage point and increasing the interface curvature there. The maximum interface deformation is practically the same in the two cases because the proximity of the anchorage point somewhat compensates for the local reduction of the interfacial tension. However, the interface curvature takes higher values in the presence of the surfactant monolayer.

There is a thin surfactant concentration boundary layer next to the interface due to the large value of the Peclet number. The surfactant depletion on the left-hand side of the interface produces a net flux of surfactant molecules from the bulk to the interface. In contrast, the surfactant accumulation on the right side of the interface reverses the flux: Molecules desorb from the interface and move to the sublayer. In this region, the surfactant concentration does not exhibit a monotonic dependency

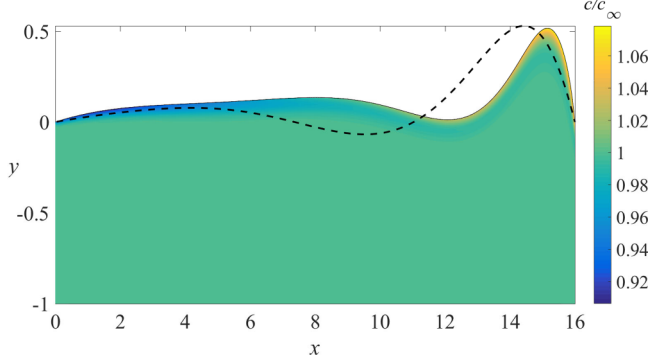


FIG. 3. Interface deformation and surfactant volume concentration  $c(x, y)$  of the base flow for  $\{\rho = 1.72, \mu = 0.5, \text{Oh} = 0.00141, \text{Ca} = 0.00681, q = 1; \text{Pe} = \text{Pe}_s = 3.54 \times 10^6, k_a = 5.96 \times 10^{-6}, k_d = 5.37 \times 10^{-9}, \text{Ma} = 0.225, c_\infty = 0.0055\}$ . The dashed line is the interface deformation in the absence of surfactant for the same values of  $\rho, \mu, \text{Oh}, q$ , and  $\text{Ca}$ .

upon the distance from the interface. In fact, there is a layer below the interface where the surfactant concentration is smaller than that of the bulk  $c = 1$ . This effect is caused by the convection parallel to the interface of the low surfactant concentration found on the left-hand side.

The results shown in Fig. 3 were obtained for a realistic value of the Peclet number. This parameter is expected not to influence the system dynamics only if  $\varepsilon \equiv \hat{k}_d \hat{W} \hat{\Gamma}_\infty / (\hat{c}_\infty \hat{D}_1) \ll 1$  [26]. In our simulations,  $\varepsilon = 2.2$  and, therefore, diffusion may affect the system stability. As can be observed in Fig. 4(a), the Peclet number influences the thickness of the boundary layer next to the interface and, to a lesser extent, the value of surfactant volume concentration. However, neither the surfactant surface concentration nor the interface deformation is significantly affected by the Peclet number [Fig. 4(b)]. In other words, the base flow does not significantly change when the diffusion coefficient is increased by two orders of magnitude except for the surfactant distribution next to the interface.

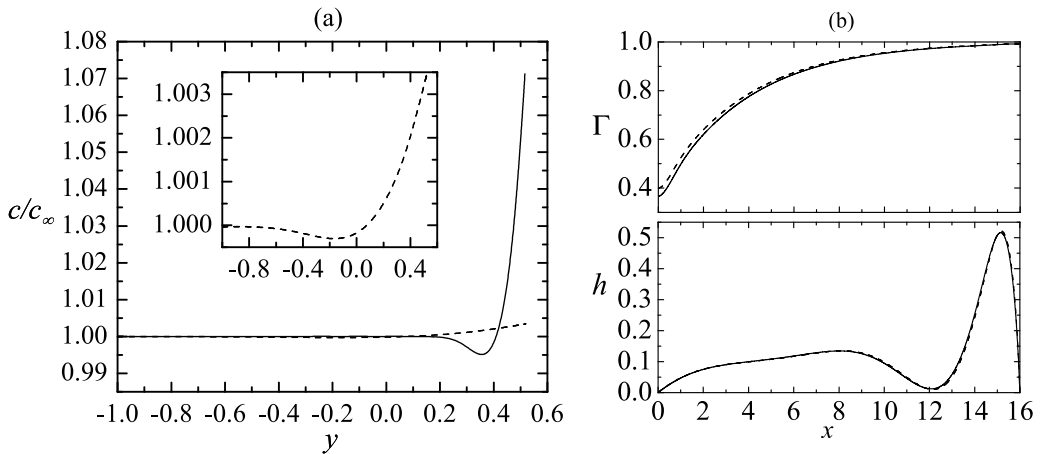


FIG. 4. (a) Surfactant volume concentration  $c(x, y)$  at  $x = 15.16$ . (b) Interface contour  $h(x)$  and surfactant surface concentration  $\Gamma(x)$ . The results were calculated for  $\text{Pe} = \text{Pe}_s = 3.54 \times 10^6$  (solid line) and  $3.54 \times 10^4$  (dashed line) and for  $\{\rho = 1.72, \mu = 0.5, \text{Oh} = 0.00141, \text{Ca} = 0.00681, q = 1; k_a = 5.96 \times 10^{-6}, k_d = 5.37 \times 10^{-9}, \text{Ma} = 0.225, c_\infty = 0.0055\}$ .



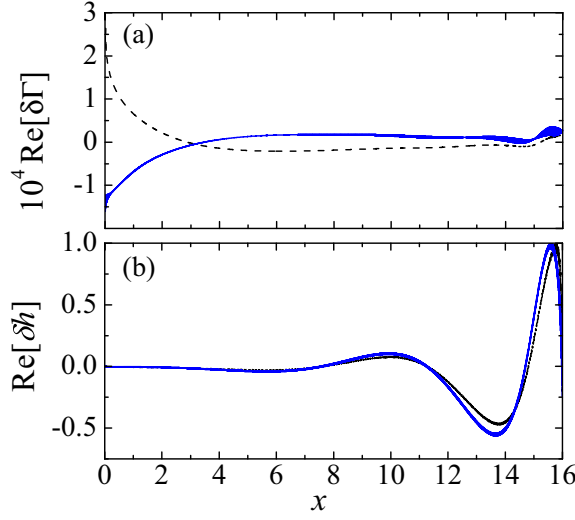


FIG. 5. Perturbation of (a) the interface contour  $\text{Re}[\delta h(x)]$  and (b) the surfactant surface concentration  $\text{Re}[\delta \Gamma(x)]$  for  $\text{Pe} = \text{Pe}_s = 3.54 \times 10^6$  (solid blue lines) and  $3.54 \times 10^4$  (dashed black lines). The results were calculated for  $\{\rho = 1.72, \mu = 0.5, \text{Oh} = 0.00141, \text{Ca} = 0.00681, q = 1; k_a = 5.96 \times 10^{-6}, k_d = 5.37 \times 10^{-9}, \text{Ma} = 0.225, c_\infty = 0.0055\}$ .

The noticeable effect of the surfactant convection can be appreciated in the distribution  $\Gamma(x)$ , which considerably increases downstream and reaches its maximum value  $\Gamma \simeq 1$  ( $\hat{\Gamma} \simeq \hat{\Gamma}_\infty$ ) at the right-hand anchor point [Fig. 4(b)]. Since  $k_a \gg k_d$ , we obtain  $\Gamma \approx \mathcal{O}(1)$  over the whole interface despite the tiny amount of surfactant (in terms of the critical micellar concentration) dissolved in phase 1 ( $c = 0.0055$ ). It should be noted that, for the surfactant properties considered in our simulations, that amount of surfactant corresponds to  $\Gamma = 0.859$  at equilibrium, a value relatively close to the maximum packing density.

As explained above, both the concentration and the concentration gradient increase next to the interface when the surfactant diffusion coefficient is decreased. However, the other quantities of the *steady* base flow remain essentially the same. One may wonder if the *unsteady* perturbation is also insensitive to the  $\text{Pe}$  and  $\text{Pe}_s$  values. Figure 5 shows the perturbations of the interface contour and surfactant surface concentration corresponding to the dominant mode of the base flow described above. There is a slight influence of  $\text{Pe}$  on  $\delta h$ . The influence on  $\delta \Gamma$  is noticeable in relative terms. However, the surfactant surface concentration  $\Gamma$  remains practically unperturbed ( $\delta \Gamma \ll \Gamma$ ), implying that the interfacial tension profile established in the steady base flow remains practically constant during the evolution of the dominant mode. Therefore, the effect of the Peclet number on  $\delta \Gamma$  hardly alters that evolution. In fact, the critical capillary numbers for instability for  $\text{Pe} = 3.54 \times 10^6$  and  $3.54 \times 10^4$  differ by less than 1.15%. The numerical fluctuations decrease as  $\text{Pe}$  decreases even though the grid spatial resolution is much smaller for  $\text{Pe} = 3.54 \times 10^4$ . For this reason, we hereafter consider  $\text{Pe} = 3.54 \times 10^4$  in our simulations.

In the absence of surfactant, the flow becomes unstable due to the difference between the hydrostatic pressure on the two sides of the interface [8]. The response of the system is more complex when a surfactant is dissolved in phase 1. However, the instability is still associated to some extent with the mismatch between the hydrostatic pressures on the two sides of the interface at the junction inlet. This pressure difference is proportional to the product  $\mu q$  because the flow is developed in the channels. Therefore, one can expect the system behavior to be practically the same if  $\mu q$  takes the same value. We have verified this expectation by comparing the results for  $(\mu = 0.9, q = 0.8)$  and  $(\mu = 0.72, q = 1)$ . The critical capillary number, interface deformation,

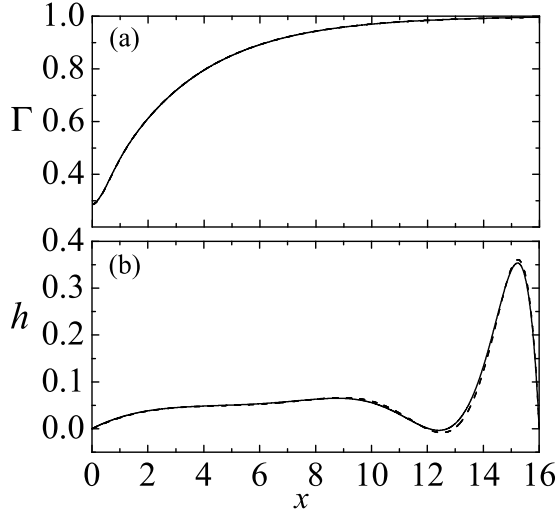


FIG. 6. (a) Surfactant surface concentration  $\Gamma(x)$  and (b) interface deformation  $h(x)$  for  $\{\rho = 1.72, \text{Oh} = 0.00141; Ca = 0.00703, \text{Pe} = \text{Pe}_s = 3.54 \times 10^4, k_a = 5.96 \times 10^{-6}, k_d = 5.37 \times 10^{-9}, \text{Ma} = 0.225, c_\infty = 0.0055\}$  and  $(\mu = 0.9, q = 0.8)$  (solid lines) and  $(\mu = 0.72, q = 1)$  (dashed lines).

and surfactant concentration were practically the same in the two cases (Fig. 6). Hereafter, we will set  $q = 1$  in all the simulations and focus on the influence of  $\mu$  on the base flow and the critical capillary number  $Ca^*$ .

When there is a mismatch between the two viscosities, the jump of hydrostatic pressures across the interface increases almost linearly with the capillary number (the injection flow rate). This explains why the maximum steady-state interface deformation  $\max(|h(x)|)$  is approximately proportional to  $Ca$  (Fig. 7). When the maximum interface deformation exceeds a critical value, the flow becomes unstable due to the growth of the dominant perturbation. The maximum deformation withstood by the interface increases as the viscosity ratio decreases. In other words, larger stable deformations can be obtained for smaller  $\mu$ . This occurs even though the critical capillary number

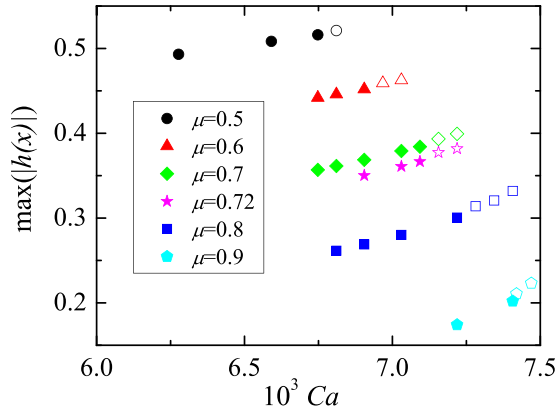


FIG. 7. Maximum interface deformation,  $\max(|h(x)|)$ , as a function of the capillary number  $Ca$  for different values of the viscosity ratio  $\mu$  for  $\{\rho = 1.72, \text{Oh} = 0.00141, q = 1; \text{Pe} = \text{Pe}_s = 3.54 \times 10^4, k_a = 5.96 \times 10^{-6}, k_d = 5.37 \times 10^{-9}, \text{Ma} = 0.225, c_\infty = 0.0055\}$  (circles). The solid and open symbols correspond to stable and unstable base flows, respectively.

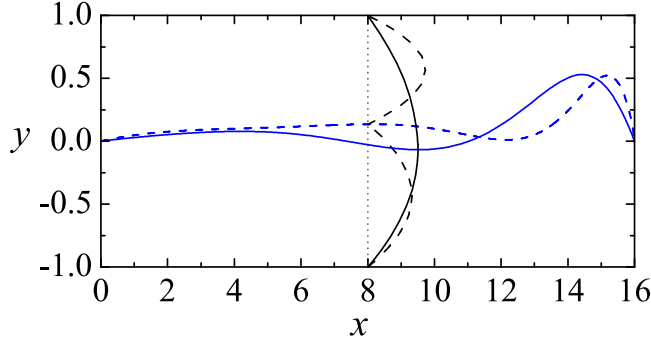


FIG. 8. Shape of the velocity profile  $u(y)$  at  $x = 8$  for  $c_\infty = 0$  (solid line) and  $c_\infty = 0.0055$  (dashed line). The results were calculated for  $\{\rho = 1.72, \mu = 0.5, \text{Oh} = 0.00141, Ca = 0.00681, q = 1; \text{Pe} = \text{Pe}_s = 3.54 \times 10^4, k_d = 5.96 \times 10^{-6}, k_d = 5.37 \times 10^{-9}, \text{Ma} = 0.225\}$ . The blue lines correspond to the interface positions.

decreases as  $\mu$  decreases (Fig. 7). The quantity  $\max(|h(x)|)$  depends almost linearly on  $Ca$  even when the critical capillary number is exceeded. In fact, the critical point is surpassed without any qualitative indication on the solution. This illustrates the importance of conducting the linear stability analysis to ensure that the steady solution corresponds to an experimentally available state.

To better understand the role played by the surfactant monolayer, we now compare the results calculated with and without surfactant. The following simple scaling analysis of the conservation Eq. (15) reveals that the surfactant monolayer immobilizes the interface. Both  $\Gamma_t$  and  $v^n$  ( $v^n$  is the normal velocity to the interface) vanish in the steady base flow, while the surfactant net flux  $\mathcal{J}$  and surface diffusion are at most of the order of  $10^{-4}$ . Therefore, and according to Eq. (15), the net superficial flux of surfactant,  $\phi_x(x)$  ( $\phi \equiv \Gamma v^t$  and  $v^t$  is the tangential velocity along the interface), is practically zero over the interface. In addition, the anchorage condition ensures that  $v^t = 0$  at the two interface ends  $x = 0$  and  $L_m$ , and, therefore,  $\phi = 0$  at those two points. Since  $\phi(0) = \phi(L_m) = 0$  and  $\phi_x(x) \simeq 0$ ,  $\phi(x)$  must take very small values along the interface. The surfactant density  $\Gamma(x)$  takes values of order unity (Fig. 4). Therefore,  $v^t(x) \simeq 0$  over the whole interface.

The above conclusion means that a Poiseuille-like velocity profile is established on the two sides of the interface (Fig. 8), which contrasts with the velocity distribution in the absence of surfactant. Marangoni stress provides the force necessary to immobilize the interface. Without this force, the interface immobilization is not feasible, and the conservation Eq. (15) cannot be verified. In fact, if we “turn off” the Marangoni stress term  $-\gamma_x \sqrt{1 + h_x^2}$  in Eq. (12), then the numerical code cannot converge to a proper solution.

We showed in Fig. 3 that the addition of surfactant displaces the interfacial deformation towards the right-hand anchor point. There is a fundamental difference between the instability with and without surfactants. The instability is caused by an oscillatory mode ( $\omega_r \neq 0$ ) in the absence of surfactant (supercritical Hopf bifurcation). In contrast, the critical frequency vanishes when a surfactant is added to phase 1 (Fig. 9), i.e., the system becomes unstable due to the growth of a nonoscillatory perturbation. In the absence of surfactant, the oscillation frequency  $\omega_r \text{Oh}^{-1/2}$  measured in terms of the inertio-capillary time  $t_{ic} = (\rho_1 \dot{W}^3 / \dot{\gamma}_c)^{1/2}$  is of the order unity, which suggests that the oscillation is produced by the interfacial tension restoring force.

The difference between the critical modes with and without surfactant can be appreciated in Fig. 10, where the interface perturbation  $\delta h(x)$  is plotted for the two cases. This function has been normalized so that the area enclosed in the two cases is the same. The extra-reduction of the interfacial tension next to the right-hand end enhances the interface protrusion in that region, destabilizing the base flow.

The system becomes unstable for capillary numbers above a critical value. Figure 11 compares the critical capillary numbers with and without surfactant. We could not calculate  $Ca^*$  for larger

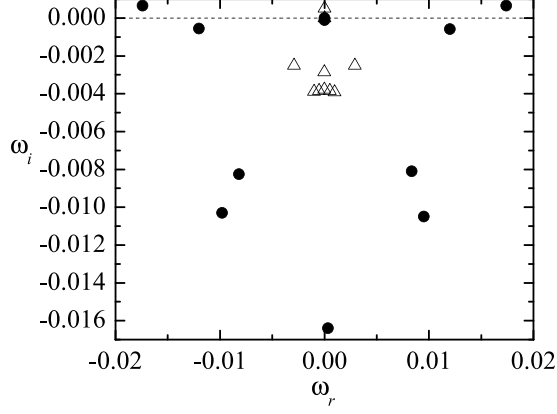


FIG. 9. Growth rate  $\omega_i$  and frequency  $\omega_r$  of the eigenvalues with  $\omega_i \geq -0.0164$  for ( $c_\infty = 0$ ,  $Ca = 0.0248$ ) (solid symbols) and ( $c_\infty = 0.0055$ ,  $Ca = 0.00728$ ) (open symbols). The results were calculated for  $\{\rho = 1.72$ ,  $\mu = 0.8$ ,  $Oh = 0.00141$ ,  $q = 1$ ;  $Pe = Pe_s = 3.54 \times 10^4$ ,  $k_a = 5.96 \times 10^{-6}$ ,  $k_d = 5.37 \times 10^{-9}$ ,  $Ma = 0.225\}$ .

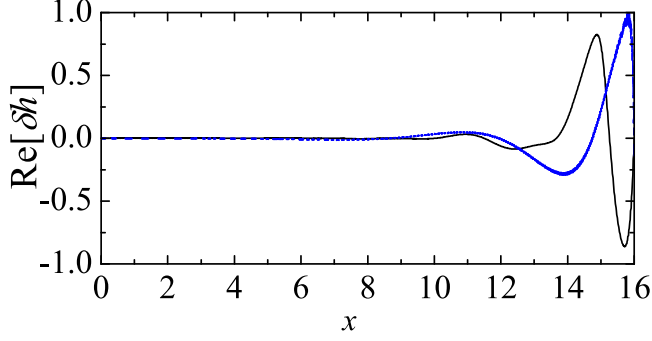


FIG. 10. Interface perturbation  $Re[\delta h(x)]$  for the critical conditions ( $c_\infty = 0$ ,  $Ca = 0.0248$ ) (solid line) and ( $c_\infty = 0.0055$ ,  $Ca = 0.00728$ ) (dashed line). The results were calculated for  $\{\rho = 1.72$ ,  $\mu = 0.8$ ,  $Oh = 0.00141$ ,  $q = 1$ ;  $Pe = Pe_s = 3.54 \times 10^4$ ,  $k_a = 5.96 \times 10^{-6}$ ,  $k_d = 5.37 \times 10^{-9}$ ,  $Ma = 0.225\}$ .  $Re[\delta h(x)]$  has been normalized so that the area enclosed in the two cases is the same.

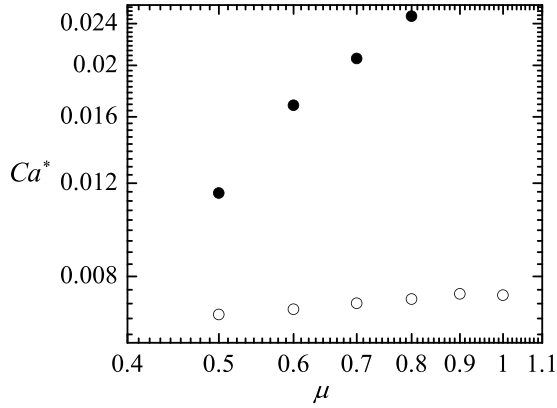


FIG. 11. Critical capillary number  $Ca^*$  as a function of the viscosity ratio  $\mu$  for  $\{\rho = 1.72$ ,  $Oh = 0.00141$ ,  $q = 1$ ;  $Pe = Pe_s = 3.54 \times 10^4$ ,  $k_a = 5.96 \times 10^{-6}$ ,  $k_d = 5.37 \times 10^{-9}$ ,  $Ma = 0.225\}$  and for  $c_\infty = 0$  (solid symbols) and 0.0055 (open symbols).

values of  $\mu$  due to the high spatial resolution demanded by the simulation as the capillary number increases. In the absence of surfactant,  $Ca^*$  significantly increases as  $\mu \rightarrow 1$ , which indicates that the instability is linked to the difference between the pressure drop across the inlet ducts. The system behavior in the presence of surfactant is drastically different. The system is much more unstable, and the critical capillary number hardly depends on the viscosity ratio. In fact, the surfactant monolayer destabilizes the interface for small capillary numbers even under perfect symmetry conditions ( $\mu = q = 1$ ). This result has obvious practical implications: Imperfect separation is expected at the outlet of the microfluidic device if one of the phases carries a surfactant or surface-active impurities.

We have verified that the curve  $Ca^*(\mu)$  in Fig. 11 is almost symmetric with respect to  $\mu = 1$  on a logarithmic scale, i.e.,  $Ca^*(\mu) \simeq Ca^*(\mu^{-1})$ . In other words, the stability limit is practically the same when the two phases are exchanged ( $1 \leftrightarrow 2, \mu \leftrightarrow \mu^{-1}$ ). This indicates that (i) the density ratio and Ohnesorge number play a negligible role in the instability, and (ii) the system stability is almost independent of the phase in which the surfactant is dissolved. As expected, the system behavior depends on the surfactant monolayer composition, regardless of the liquid phase from which the surfactant molecules come.

The interfacial tension is a stabilizing factor. The capillary number was defined in terms of the corresponding equilibrium interfacial tension. Therefore, the decrease in  $Ca^*$  cannot be attributed to a *global* reduction of the interfacial tension. In contrast, the *local* soluto-capillarity effect does enhance the flow instability. The surfactant accumulation at the downstream end of the interface reduces the interfacial tension below its equilibrium value in that critical region, where the interface deformation and curvature caused by the dominant mode reaches the maximum value (Fig. 5). This extra-reduction of the interfacial tension due to the surfactant accumulation destabilizes the system. To test this hypothesis, we have applied the value of the interfacial tension at equilibrium to all the interface points when calculating the critical mode (not the base flow). We verified that the growth rate of that mode decreases, i.e., the system becomes more stable. Therefore, the instability must be attributed to the uneven distribution of the interfacial tension over the interface.

The Marangoni convention is expected to stabilize the system because it opposes the gradient of surfactant concentration caused by the coflowing stream. To test this expectation, we turned off the Marangoni stress  $-\gamma_x \sqrt{1 + h_x^2}$  in Eq. (12) when calculating the critical mode (not the base flow) and verified that the growth rate of that mode increases. This means that the system becomes more stable when the Marangoni stress is considered.

## V. CONCLUDING REMARKS

We have studied the effect of a soluble surfactant on the linear stability of two-phase flows in a finite-length channel. Our results show that a very small amount of surfactant dissolved in one of the phases considerably destabilizes the system. Due to the disparity between the dimensionless surfactant adsorption and desorption constants, the surfactant surface concentration takes values of the order of the maximum packing density over the whole interface. The streams convect the surfactant molecules towards the right-hand end of the interface, where the maximum deformation is produced even in the absence of surfactant. The surface concentration in that region becomes slightly lower than the maximum packing density. The interfacial tension profile established by the base flow hardly changes during the growth of the critical mode. The local decrease in the interfacial tension increases both the steady deformation and the deformation caused by the critical perturbation next to the right-hand end of the interface. This effect considerably enhances the instability, which translates into a sharp reduction of the critical capillary number. Very small critical capillary numbers are obtained in the presence of surfactant, even if the base flow is perfectly symmetric ( $\mu = q = 1$ ).

Other conclusions of our study are the following. The bulk diffusion coefficient hardly affects the base flow and its stability. This implies that accurate predictions can be obtained with significantly larger values of that parameter, which considerably simplifies the simulations. The maximum interface deformation is approximately proportional to the capillary number. Larger stable deformations

are obtained for smaller values of the viscosity ratio. The surfactant monolayer suppresses the interface motion, producing a Poiseuille-like velocity profile in the two phases. The instability is caused by an oscillatory mode in the absence of surfactant, while the system becomes unstable due to the growth of a nonoscillatory perturbation when the surfactant is added.

The experimental systems typically have significant 3D and exit effects, which hinders a quantitative comparison between those experiments and 2D simulations. Nevertheless, we have observed in our preliminary experiments that adding a surfactant decreases the period of the instability, which at least is qualitatively consistent with the larger growth rates of the unstable modes observed in the simulations.

It is well known that an infinite two-layer parallel flow is unstable under long-wavelength perturbations. Kalogirou and Blyth [23] have shown that a sufficiently soluble surfactant stabilizes the flow for  $\mu < \rho^2$ . In this case, solubility redistributes the surfactant over the interface and partially suppresses the destabilizing Marangoni stress, which stabilizes the system under long-wave and midwave perturbations. The properties of the liquids and the channel width in the present work considerably differ from those in Ref. [23]. Therefore, a quantitative comparison is not feasible. Nevertheless, we may state that, according to the results by Kalogirou and Blyth [23], the value of the solubility parameter  $R_b = \hat{k}_a/(\hat{k}_d 2\hat{W}) \simeq 198$  in our simulations seems too large for the surfactant to stabilize the perturbations allowed in our systems, i.e., those with wavelengths smaller than the channel length.

In any case, the behavior of the finite-length microchannel is fundamentally different from that of the infinite case. The surfactant accumulation in the microchannel's downstream end reduces the interfacial tension in that region. The local decrease in the interfacial tension increases the deformation caused by the critical perturbation, which considerably enhances the instability. Marangoni convection stabilizes the flow (contrary to what occurs in the infinite case) because it opposes the accumulation of surfactant in the downstream end.

The critical eigenmode is oscillatory ( $\omega_r \neq 0$ ) for a clean interface and becomes nonoscillatory ( $\omega_r = 0$ ) with the addition of a surfactant. The linear stability analysis captures only the initial growth of the interface deformation. The oscillatory or nonoscillatory character of the critical eigenmode is not, in principle, linked to the periodic shedding of drops, which is a nonlinear phenomenon. In fact, this phenomenon happens not only in the absence of a surfactant but also in the presence of it, as observed in our preliminary experiments.

## ACKNOWLEDGMENTS

This research has been supported by the Spanish Ministry of Economy, Industry, and Competitiveness under Grants No. DPI2016-78887 and No. PID2019-108278RB, by Junta de Extremadura under Grant No. GR18175, and by Junta de Andalucía under Grant No. P18-FR-3623.

- 
- [1] J. Burns and C. Ramshaw, Development of a microreactor for chemical production, *Chem. Eng. Res. Des.* **77**, 206 (1999).
  - [2] D. A. Wenn, J. E. Shaw, and B. Mackenzie, A mesh microcontactor for 2-phase reactions, *Lab Chip* **3**, 180 (2003).
  - [3] T. Maruyama, J.-I. Uchida, T. Ohkawa, T. Futami, K. Katayama, K.-I. Nishizawa, K.-I. Sotowa, F. Kubota, N. Kamiya, and M. Goto, Enzymatic degradation of *p*-chlorophenol in a two-phase flow microchannel system, *Lab Chip* **3**, 308 (2003).
  - [4] S.-X. Meng, L.-H. Xue, C.-Y. Xie, R.-X. Bai, X. Yang, Z.-P. Qiu, T. Guo, Y.-L. Wang, and T. Meng, Enhanced enzymatic reaction by aqueous two-phase systems using parallel-laminar flow in a double Y-branched microfluidic device, *Chem. Eng. J.* **335**, 392 (2018).
  - [5] P. F. Jahromi, J. Karimi-Sabet, and Y. Amini, Ion-pair extraction-reaction of calcium using Y-shaped microfluidic junctions: An optimized separation approach, *Chem. Eng. J.* **334**, 2603 (2018).

- [6] M. Surmeian, M. N. Slyadnev, H. Hisamoto, A. Hibara, K. Uchiyama, and T. Kitamori, Three-layer flow membrane system on a microchip for investigation of molecular transport, *Anal. Chem.* **74**, 2014 (2002).
- [7] T. Maruyama, H. Matsushita, J.-I. Uchida, F. Kubota, N. Kamiya, and M. Goto, Liquid membrane operations in a microfluidic device for selective separation of metal ions, *Anal. Chem.* **76**, 4495 (2004).
- [8] P. R. Kaneelil, A. A. Pahlavan, M. A. Herrada, K. LeRoy, K. Stengel, S. Warner, A. M. Galea, and H. A. Stone, Symmetry breaking of a parallel two-phase flow in a finite length channel, *Phys. Rev. Fluids* **7**, 033904 (2022).
- [9] C.-S. Yih, Instability due to viscosity stratification, *J. Fluid Mech.* **27**, 337 (1967).
- [10] R. Dreyfus, P. Tabeling, and H. Willaime, Ordered and Disordered Patterns in Two-Phase Flows in Microchannels, *Phys. Rev. Lett.* **90**, 144505 (2003).
- [11] P. Guillot and A. Colin, Stability of parallel flows in a microchannel after a T junction, *Phys. Rev. E* **72**, 066301 (2005).
- [12] A. Hibara, M. Nonaka, H. Hisamoto, K. Uchiyama, Y. Kikutani, M. Tokeshi, and T. Kitamori, Stabilization of liquid interface and control of two-phase confluence and separation in glass microchips by utilizing octadecylsilane modification of microchannels, *Anal. Chem.* **74**, 1724 (2002).
- [13] A. Aota, A. Hibara, and T. Kitamori, Pressure balance at the liquid-liquid interface of micro countercurrent flows in microchips, *Anal. Chem.* **79**, 3919 (2007).
- [14] D. Ciceri, J. M. Perera, and G. W. Stevens, The use of microfluidic devices in solvent extraction, *J. Chem. Technol. Biotechnol.* **89**, 771 (2014).
- [15] P. F. Jahromi, J. Karimi-Sabet, Y. Amini, and H. Fadaei, Pressure-driven liquid-liquid separation in Y-shaped microfluidic junctions, *Chem. Eng. J.* **328**, 1075 (2017).
- [16] Y.-M. Tricot, *Surfactants: Static and Dynamic Surface Tension*, (Chapman and Hall, London, 1997), pp. 100–136.
- [17] Y. He, P. Yazhgur, A. Salonen, and D. Langevin, Adsorption-desorption kinetics of surfactants at liquid surfaces, *Adv. Colloid Interface Sci.* **222**, 377 (2015).
- [18] C.-H. Chang and E. I. Franses, Adsorption dynamics of surfactants at the air/water interface: A critical review of mathematical models, data, and mechanisms, *Colloids Surf. A* **100**, 1 (1995).
- [19] Z. A. Zell, A. Nowbahar, V. Mansard, L. G. Leal, S. S. Deshmukh, J. M. Mecca, C. J. Tucker, and T. M. Squires, Surface shear inviscidity of soluble surfactants, *Proc. Natl. Acad. Sci. USA* **111**, 3677 (2014).
- [20] A. Ponce-Torres, M. Rubio, M. A. Herrada, J. Eggers, and J. M. Montanero, Influence of the surface viscous stress on the pinch-off of free surfaces loaded with nearly-inviscid surfactants, *Sci. Rep.* **10**, 16065 (2020).
- [21] M. A. Herrada, A. Ponce-Torres, M. Rubio, J. Eggers, and J. M. Montanero, Stability and tip streaming of a surfactant-loaded drop in an extensional flow. Influence of surface viscosity, *J. Fluid Mech.* **934**, A26 (2022).
- [22] R. V. Craster, O. K. Matar, and D. T. Papageorgiou, Breakup of surfactant-laden jets above the critical micelle concentration, *J. Fluid Mech.* **629**, 195 (2009).
- [23] A. Kalogirou and M. G. Blyth, The role of soluble surfactants in the linear stability of two-layer flow in a channel, *J. Fluid Mech.* **873**, 18 (2019).
- [24] M. A. Herrada and J. M. Montanero, A numerical method to study the dynamics of capillary fluid systems, *J. Comput. Phys.* **306**, 137 (2016).
- [25] A. Ponce-Torres, N. Rebollo-Muñoz, M. A. Herrada, A. M. Gañán-Calvo, and J. M. Montanero, The steady cone-jet mode of electrospraying close to the minimum volume stability limit, *J. Fluid Mech.* **857**, 142 (2018).
- [26] C. D. Eggleton and K. J. Stebe, An adsorption-desorption-controlled surfactant on a deforming droplet, *J. Colloid Interface Sci.* **208**, 68 (1998).